Journal of Engineering Mathematics **28**: 483–499, 1994.

Effects of transpiration on free convection in an annulus between concentric porous spheres

S.D. GULWADI and A.F. ELKOUH

Department of Mechanical and Industrial Engineering, Marquette University, Milwaukee, Wisconsin 53233, U.S.A.

Received 22 June 1993; accepted in revised form 28 March 1994

Abstract. An analysis is presented to study the effects of transpiration on free convection in an annulus between concentric porous spheres. A regular perturbation technique is applied to solve the steady-state Navier–Stokes equations of motion and the energy equation, whereby the stream-function and temperature are expanded in the form of power series in terms of the Rayleigh number Ra, and injection/suction Reynolds number Re. The analytical solution is valid for small values of Ra and Re, and all values of the Prandtl number Pr. A finite-difference solution of the governing steady-state equations of motion and energy is also provided. The range of validity of the analytical solution is determined by comparison with the numerical solution. Plots of the flow patterns, velocity distributions, temperature profiles, local and overall heat transfer rates are presented for $Pr = 0.7$ and different values of Re, Ra, and the radius ratio λ. Results are shown over a range of values of Ra and Re such that the effects of mixed convection in the annulus can be clearly observed.

1. Introduction

Flow and heat transfer next to porous boundaries is of practical significance in many areas of engineering. Examples include applications in filtration, gaseous diffusion, lubrication, and oil processing and recovery. Fluid injection or suction through permeable boundaries is an effective method of controlling heat transfer in channels and enclosures. Heat transfer in spherical enclosures has been extensively investigated due to its relevance in nuclear reactor engineering, and spherical fluid storage systems. In this study, the effects of transpiration on natural convection in an annulus between concentric porous spheres are analyzed. The interactions between the radial flow-field (due to injection/suction at the porous spherical walls), and free convection flow (created by the temperature difference between the porous spheres) are studied due to their importance in the design of spherical fluid storage systems. In these applications, transpiration cooling is used to regulate the rate of heat transfer.

Free convection in an annulus between concentric non-porous spheres has been investigated by many researchers, and only studies with relevance to this investigation are reported here. Mack and Hardee [1] developed a perturbation solution whereby they expanded the stream-function and temperature in the form of power series in terms of the Rayleigh number Ra. Singh and Chen [2] extended the study to higher values of the Rayleigh number by using a series solution in terms of Legendre polynomials and Gegenbauer functions. Numerical solutions to this problem have been obtained by Astill et al. [3], Caltagirone et al. [4], Ingham [5], and more recently by Garg [6]. In these studies, finite-difference techniques were utilized to solve the unsteady equations of motion and energy, and the final steady-state results were presented for large values of the Rayleigh number. Experimental investigations of free convection in a spherical annulus have been conducted by Bishop et al. [7], Scanlan et al. [8], and Yin et al. [9]. Their results include flow patterns, temperature profiles, and heat transfer correlations over a wide range of Rayleigh numbers, and for different values of the Prandtl number Pr, and radius ratio λ.

Heat transfer about a rotating porous sphere in an infinite medium and with injection/suction at the sphere's boundary has been analyzed in conjunction with fluid flow studies by Lien et al. [10], and more recently by Hatzikonstantinou [11]. In both cases, finite-difference schemes were used to solve the boundary layer equations, whereby Lien et al. [10] studied the steady laminar mixed free-forced convection about a rotating porous sphere, and Hatzikonstantinou [11] analyzed the unsteady laminar mixed convection about a rotating porous sphere. Studies of flow in an annulus between rotating porous spheres and with injection/suction at the spherical walls have been conducted by Gulwadi et al. [12]. They employed a perturbation technique to solve the Navier–Stokes equations of motion and also used a finite-difference solution to validate their analytical results.

The effects of transpiration on free convection on a vertical porous plate and on a porous cone have been analyzed by several researchers [13–18]. However, a review of the literature reveals that there have been no theoretical or experimental studies of the effects of transpiration on free convection in an annulus between concentric porous spheres. In this study, an analytical solution of the steady-state Navier–Stokes equations of motion and the energy equation is obtained by employing a regular perturbation technique. Solutions for the stream-function and temperature are obtained in the form of power series expansions in terms of the Rayleigh number Ra, and injection/suction Reynolds number Re. The analytical solution is valid for small values of Ra and Re, and all values of the Prandtl number Pr. A numerical solution of the steady-state Navier–Stokes equations of motion and the energy equation is obtained by employing a finite-difference scheme. The range of validity of the analytical solution is determined by comparison with the numerical solution. Results for the flow patterns, velocity distributions, temperature profiles, local and overall heat transfer rates are presented for $Pr = 0.7$ and various values of the Rayleigh number Ra, injection/suction Reynolds number Re, and radius ratio λ.

2. Basic equations and their solutions

The laminar axially-symmetric motion of an incompressible Newtonian fluid in an annulus between concentric porous spheres is considered (Fig. 1). The inner porous sphere of radius $\bar{R}_1$ is maintained at a uniform temperature $\bar{T}_1$, while the outer porous sphere of radius $\bar{R}_2$ is at a uniform temperature $\bar{T}_2$. Fluid can be uniformly injected or sucked at the porous spherical walls, and the rate of injection or suction is based on the uniform radial velocity component $\bar{V}_{w1}$ at the inner porous boundary. The spheres are stationary and a uniform gravitational field acts vertically downward parallel to the fixed axis of the porous spheres. The geometry of the annulus is characterized by the radius ratio $\lambda = \bar{R}_1/\bar{R}_2$; and the spherical coordinates used are the meridional angle θ, azimuthal angle ϕ, and the radial coordinate r, where $r = \bar{r}/\bar{R}_1$. All terms denoted by a bar represent dimensional quantities.

The temperature difference between the inner and outer porous spheres gives rise to a free convection flow pattern in the annulus. The parameter governing the buoyancy-induced flow is given by the Rayleigh number $Ra = \bar{g}\bar{\beta}\bar{R}_1^3(\bar{T}_1 - \bar{T}_2)/\bar{\nu}\bar{\alpha}$; where $\bar{\beta}$, $\bar{\nu}$, and $\bar{\alpha}$ are the thermal expansion coefficient, kinematic viscosity, and thermal diffusivity of the fluid, respectively. The rate of injection or suction at the spherical porous walls is represented by the injection/suction Reynolds number $Re = \bar{V}_{w1}\bar{R}_1/\bar{\nu}$. In this study, positive values of Re are referred to as 'injection Reynolds numbers' which indicate injection at the inner sphere with suction at the outer, while negative values of Re are referred to as 'suction Reynolds

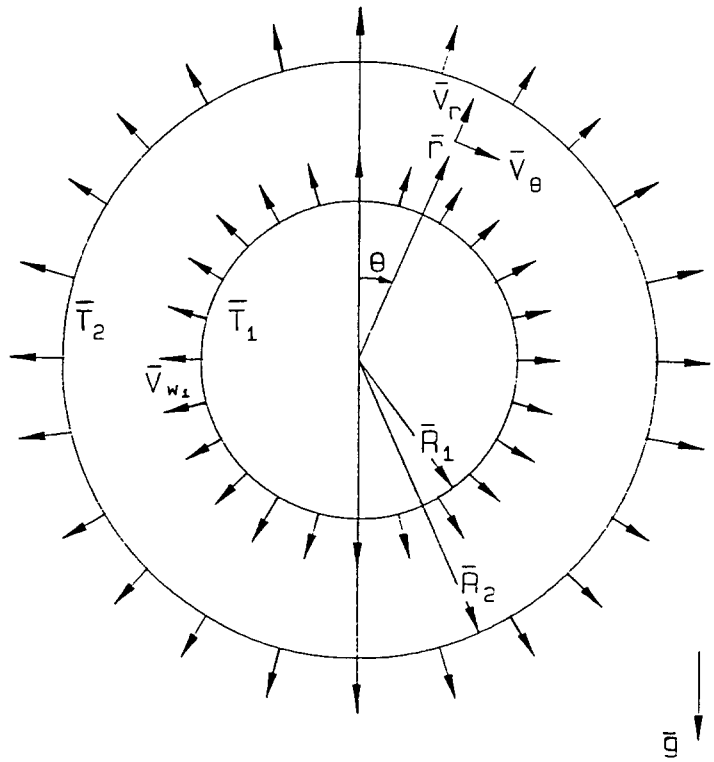

Fig. 1. Notation for flow in the spherical annulus.

numbers' and they imply the opposite. The Prandtl number defined as $Pr = \bar{\nu}/\bar{\alpha}$ represents the ratio of momentum diffusivity to thermal diffusivity, and is used to characterize the fluid in the annulus.

The dimensionless radial and meridional velocity components are expressed as $V_r = \bar{V}_r \bar{R}_1/\bar{\nu}$ and $V_\theta = \bar{V}_\theta \bar{R}_1/\bar{\nu}$, respectively. By defining a dimensionless stream-function $\psi = \bar{\psi}/\bar{R}_1\bar{\alpha}$, such that

$$V_r = \frac{1}{(Pr)r^2 \sin\theta}\frac{\partial\psi}{\partial\theta}, \quad \text{and} \quad V_\theta = -\frac{1}{(Pr)r\sin\theta}\frac{\partial\psi}{\partial r}, \tag{1}$$

the equation of continuity is satisfied. The definition of ψ given by equation (1) makes it possible to obtain a solution valid for all values of Pr.

All fluid properties are assumed constant except for the density which is modeled based on the Boussinesq approximation. Additionally, viscous dissipation terms are also neglected in the energy equation. By introducing a dimensionless temperature difference $T = (\bar{T} - \bar{T}_2)/(\bar{T}_1 - \bar{T}_2)$, and by using the definition of ψ given in equation (1), the steady-state Navier–Stokes equation of motion and the energy equation are

$$D^4\psi + \frac{\sin\theta}{(Pr)}\left[\frac{\partial\psi}{\partial r}\frac{\partial}{\partial\theta} - \frac{\partial\psi}{\partial\theta}\frac{\partial}{\partial r}\right]\left(\frac{D^2\psi}{r^2\sin^2\theta}\right) + (Ra)\sin\theta\left[r\sin\theta\frac{\partial T}{\partial r} + \cos\theta\frac{\partial T}{\partial\theta}\right] = 0, \tag{2}$$

and

$$\nabla^2 T - \frac{1}{r^2 \sin\theta}\left(\frac{\partial\psi}{\partial\theta}\frac{\partial T}{\partial r} - \frac{\partial\psi}{\partial r}\frac{\partial T}{\partial\theta}\right) = 0\,, \tag{3}$$

where:

$$D^2 \equiv \frac{\partial^2}{\partial r^2} + \frac{1}{r^2}\frac{\partial^2}{\partial\theta^2} - \frac{\cot\theta}{r^2}\frac{\partial}{\partial\theta}\,,$$

$$\nabla^2 \equiv \frac{\partial^2}{\partial r^2} + \frac{2}{r}\frac{\partial}{\partial r} + \frac{1}{r^2}\frac{\partial^2}{\partial\theta^2} + \frac{\cot\theta}{r^2}\frac{\partial}{\partial\theta}\,,$$

and

$$D^4 \equiv D^2(D^2)\,.$$

The boundary conditions on the stream-function ψ and temperature T are

$$\frac{\partial\psi}{\partial\theta}(1,\theta) = \frac{\partial\psi}{\partial\theta}(1/\lambda,\theta) = (Re\ Pr)\sin\theta\,, \tag{4.1}$$

$$\frac{\partial\psi}{\partial r}(1,\theta) = \frac{\partial\psi}{\partial r}(1/\lambda,\theta) = 0\,, \tag{4.2}$$

$$\frac{\partial\psi}{\partial\theta}(r,0) = \frac{\partial\psi}{\partial\theta}(r,\pi) = 0\,, \tag{4.3}$$

$$\frac{\partial\psi}{\partial r}(r,0) = \frac{\partial\psi}{\partial r}(r,\pi) = 0\,, \tag{4.4}$$

$$T(1,\theta) = 1,\ T(1/\lambda,\theta) = 0\,, \tag{4.5}$$

and

$$\frac{\partial T}{\partial\theta}(r,0) = \frac{\partial T}{\partial\theta}(r,\pi) = 0\,. \tag{4.6}$$

A regular perturbation technique is employed to solve the governing equations for fluid flow and energy given by equations (2) and (3), subject to the boundary conditions shown in equations (4.1–4.6). The stream-function ψ and temperature T are expressed in the form of power series expansions in terms of Ra and Re as

$$\psi = (-\cos\theta)Re\ Pr + \sum_{i=1}^{\infty}\left(\sum_{j=0}^{\infty}\psi_{i,j}\,Re^j\right)Ra^i\,;\quad i = 1,2,3,\ldots,\quad j = 0,1,2,\ldots \tag{5}$$

and

$$T = \sum_{m=0}^{\infty}\left(\sum_{n=0}^{\infty}T_{m,n}\,Re^n\right)Ra^m\,;\quad m = 0,1,2,\ldots,\quad n = 0,1,2,\ldots \tag{6}$$

where the first term in the expression for ψ represents the radial source flow, and the other coefficients $\psi_{i,j}$ and $T_{m,n}$ are functions of r, θ, λ, and Pr only.

For the purposes of this study, the series expansions for ψ and T are truncated such that the approximate solutions for the stream-function and temperature are given by

$$\psi = (-\cos\theta)Re\,Pr + ([\psi_{1,0}] + [\psi_{1,1}]Re + [\psi_{1,2}]Re^2)(Ra) + ([\psi_{2,0}] + [\psi_{2,1}]Re)(Ra^2) + ([\psi_{3,0}])(Ra^3)\,, \tag{7}$$

and

$$T = ([T_{0,0}] + [T_{0,1}]Re + [T_{0,2}]Re^2 + [T_{0,3}]Re^3 + [T_{0,4}]Re^4) + ([T_{1,0}] + [T_{1,1}]Re + [T_{1,2}]Re^2)(Ra) + ([T_{2,0}] + [T_{2,1}]Re)(Ra^2)\,. \tag{8}$$

Substituting the expressions for ψ and T from equations (7) and (8) into equations (2) and (3), and equating coefficients of the same combination of products of powers in Ra and Re, we get a system of partial differential equations for the determination of $\psi_{i,j}$ and $T_{m,n}$. They are

$$\nabla^2 T_{0,0} = 0\,, \tag{9.1}$$

$$\nabla^2 \mathrm{T}_{0,1} = \frac{(Pr)}{r^2}\frac{\partial T_{0,0}}{\partial r}\,, \tag{9.2}$$

$$\nabla^2 \mathrm{T}_{0,2} = \frac{(Pr)}{r^2}\frac{\partial T_{0,1}}{\partial r}\,, \tag{9.3}$$

$$\nabla^2 \mathrm{T}_{0,3} = \frac{(Pr)}{r^2}\frac{\partial T_{0,2}}{\partial r}\,, \tag{9.4}$$

$$\nabla^2 \mathrm{T}_{0,4} = \frac{(Pr)}{r^2}\frac{\partial T_{0,3}}{\partial r}\,, \tag{9.5}$$

$$D^4\psi_{1,0} = -r\sin^2\theta\,\frac{\partial T_{0,0}}{\partial r}\,, \tag{9.6}$$

$$D^4\psi_{1,1} = \sin^2\theta\,\frac{\partial}{\partial r}\left(\frac{D^2\psi_{1,0}}{r^2\sin^2\theta}\right) - r\sin^2\theta\,\frac{\partial T_{0,1}}{\partial r}\,, \tag{9.7}$$

$$D^4\psi_{1,2} = \sin^2\theta\,\frac{\partial}{\partial r}\left(\frac{D^2\psi_{1,1}}{r^2\sin^2\theta}\right) - r\sin^2\theta\,\frac{\partial T_{0,2}}{\partial r}\,, \tag{9.8}$$

$$\nabla^2 T_{1,0} = \frac{1}{r^2\sin\theta}\frac{\partial\psi_{1,0}}{\partial\theta}\frac{\partial T_{0,0}}{\partial r}\,, \tag{9.9}$$

$$\nabla^2 T_{1,1} = \frac{1}{r^2\sin\theta}\left[(Pr)\sin\theta\,\frac{\partial T_{1,0}}{\partial r} + \frac{\partial\psi_{1,0}}{\partial\theta}\frac{\partial T_{0,1}}{\partial r} + \frac{\partial\psi_{1,1}}{\partial\theta}\frac{\partial T_{0,0}}{\partial r}\right], \tag{9.10}$$

$$\nabla^2 T_{1,2} = \frac{1}{r^2\sin\theta}\left[(Pr)\sin\theta\,\frac{\partial T_{1,1}}{\partial r} + \frac{\partial\psi_{1,0}}{\partial\theta}\frac{\partial T_{0,2}}{\partial r} + \frac{\partial\psi_{1,1}}{\partial\theta}\frac{\partial T_{0,1}}{\partial r} + \frac{\partial\psi_{1,2}}{\partial\theta}\frac{\partial T_{0,0}}{\partial r}\right], \tag{9.11}$$

$$D^4\psi_{2,0} = \frac{\sin\theta}{(Pr)}\frac{\partial\psi_{1,0}}{\partial\theta}\frac{\partial}{\partial r}\left(\frac{D^2\psi_{1,0}}{r^2\sin^2\theta}\right) - \left[r\sin^2\theta\,\frac{\partial T_{1,0}}{\partial r} + \sin\theta\cos\theta\,\frac{\partial T_{1,0}}{\partial\theta}\right], \tag{9.12}$$

$$D^4\psi_{2,1} = \frac{\sin\theta}{(Pr)}\left[(Pr)\sin\theta\,\frac{\partial}{\partial r}\left(\frac{D^2\psi_{2,0}}{r^2\sin^2\theta}\right) + \frac{\partial\psi_{1,0}}{\partial\theta}\,\frac{\partial}{\partial r}\left(\frac{D^2\psi_{1,1}}{r^2\sin^2\theta}\right) + \frac{\partial\psi_{1,1}}{\partial\theta}\,\frac{\partial}{\partial r}\left(\frac{D^2\psi_{1,0}}{r^2\sin^2\theta}\right) - \left[r\sin^2\theta\,\frac{\partial T_{1,1}}{\partial r} + \sin\theta\cos\theta\,\frac{\partial T_{1,1}}{\partial\theta}\right]\right], \tag{9.13}$$

$$\nabla^2 T_{2,0} = \frac{1}{r^2\sin\theta}\left[\frac{\partial\psi_{1,0}}{\partial\theta}\,\frac{\partial T_{1,0}}{\partial r} - \frac{\partial\psi_{1,0}}{\partial r}\,\frac{\partial T_{1,0}}{\partial\theta} + \frac{\partial\psi_{2,0}}{\partial\theta}\,\frac{\partial T_{0,2}}{\partial r}\right], \tag{9.14}$$

$$\nabla^2 T_{2,1} = \frac{1}{r^2\sin\theta}\left[(Pr)\sin\theta\,\frac{\partial T_{2,0}}{\partial r} + \frac{\partial\psi_{1,0}}{\partial\theta}\,\frac{\partial T_{1,1}}{\partial r} - \frac{\partial\psi_{1,0}}{\partial r}\,\frac{\partial T_{1,1}}{\partial\theta} + \frac{\partial\psi_{1,1}}{\partial\theta}\,\frac{\partial T_{1,0}}{\partial r} - \frac{\partial\psi_{1,1}}{\partial r}\,\frac{\partial T_{1,0}}{\partial\theta} + \frac{\partial\psi_{2,0}}{\partial\theta}\,\frac{\partial T_{0,1}}{\partial \mathrm{r}} + \frac{\partial\psi_{2,1}}{\partial\theta}\,\frac{\partial T_{0,0}}{\partial r}\right], \tag{9.15}$$

and

$$D^4\psi_{3,0} = \frac{\sin\theta}{(Pr)}\left[\frac{\partial\psi_{1,0}}{\partial\theta}\,\frac{\partial}{\partial r}\left(\frac{D^2\psi_{2,0}}{r^2\sin^2\theta}\right) + \frac{\partial\psi_{2,0}}{\partial\theta}\,\frac{\partial}{\partial r}\left(\frac{D^2\psi_{1,0}}{r^2\sin^2\theta}\right) - \frac{\partial\psi_{1,0}}{\partial r}\,\frac{\partial}{\partial\theta}\left(\frac{D^2\psi_{2,0}}{r^2\sin^2\theta}\right)\right] - \left[r\sin^2\theta\,\frac{\partial T_{2,0}}{\partial r} + \sin\theta\cos\theta\,\frac{\partial T_{2,0}}{\partial\theta}\right]. \tag{9.16}$$

The boundary conditions on $\psi_{i,j}$ and $T_{m,n}$ are as follows:

$$\frac{\partial\psi_{i,j}}{\partial\theta}(1,\theta) = \frac{\partial\psi_{i,j}}{\partial\theta}(1/\lambda,\theta) = 0 \quad \text{for all } i, j, \tag{10.1}$$

$$\frac{\partial\psi_{i,j}}{\partial r}(1,\theta) = \frac{\partial\psi_{i,j}}{\partial r}(1/\lambda,\theta) = 0 \quad \text{for all } i, j, \tag{10.2}$$

$$\frac{\partial\psi_{i,j}}{\partial\theta}(r,0) = \frac{\partial\psi_{i,j}}{\partial\theta}(r,\pi) = 0 \quad \text{for all } i, j, \tag{10.3}$$

$$\frac{\partial\psi_{i,j}}{\partial r}(r,0) = \frac{\partial\psi_{i,j}}{\partial r}(r,\pi) = 0 \quad \text{for all } i, j, \tag{10.4}$$

$$T_{0,0}(1,\theta) = 1,\ T_{m,n}(1,\theta) = 0 \quad \text{for all other } m,n, \tag{10.5}$$

$$T_{m,n}(1/\lambda,\theta) = 0 \quad \text{for all } m, n, \tag{10.6}$$

and

$$\frac{\partial T_{m,n}}{\partial\theta}(r,0) = \frac{\partial T_{m,n}}{\partial\theta}(r,\pi) = 0 \quad \text{for all } m, n. \tag{10.7}$$

The solution for the leading term, $T_{0,0}$, in the expansion for T is expressed as

$$T_{0,0} = \left[A_1 + \frac{A_2}{r}\right], \tag{11.1}$$

where:

$$A_1 = \frac{-\lambda}{(1-\lambda)}, \quad \text{and} \quad A_2 = \frac{1}{(1-\lambda)},$$

and it provides the temperature distribution for pure conduction. By substituting for $T_{0,0}$ from equation (11.1) into the right hand side of equation (9.2), we can solve for $T_{0,1}$, whose form is given by

$$T_{0,1} = \left[\frac{A_3}{r^2} + A_4 + \frac{A_5}{r}\right](Pr), \tag{11.2}$$

where:

$$A_3 = \frac{-1}{2(1-\lambda)}, \quad A_4 = \frac{-\lambda}{2(1-\lambda)}, \quad \text{and} \quad A_5 = \frac{(1+\lambda)}{2(1-\lambda)}.$$

In a similar manner it may be shown that

$$T_{0,2} = [f_1(r, \lambda)](Pr)^2, \tag{11.3}$$

$$T_{0,3} = [f_2(r, \lambda)](Pr)^3, \tag{11.4}$$

$$T_{0,4} = [f_3(r, \lambda)](Pr)^4, \tag{11.5}$$

$$\psi_{1,0} = [f_4(r, \lambda) \sin^2\theta], \tag{11.6}$$

$$\psi_{1,1} = [f_5(r, \lambda) \sin^2\theta](Pr) + [f_6(r, \lambda) \sin^2\theta], \tag{11.7}$$

$$\psi_{1,2} = [f_7(r, \lambda) \sin^2\theta](Pr)^2 + [f_8(r, \lambda) \sin^2\theta](Pr) + [f_9(r, \lambda) \sin^2\theta], \tag{11.8}$$

$$T_{1,0} = [f_{10}(r, \lambda) \cos\theta], \tag{11.9}$$

$$T_{1,1} = [f_{11}(r, \lambda) \cos\theta](Pr) + [f_{12}(r, \lambda) \cos\theta], \tag{11.10}$$

$$T_{1,2} = [f_{13}(r, \lambda) \cos\theta](Pr)^2 + [f_{14}(r, \lambda) \cos\theta](Pr) + [f_{15}(r, \lambda) \cos\theta], \tag{11.11}$$

$$\psi_{2,0} = [f_{16}(r, \lambda) \sin^2\theta \cos\theta] + [f_{17}(r, \lambda) \sin^2\theta \cos\theta]\frac{1}{(Pr)}, \tag{11.12}$$

$$\psi_{2,1} = [f_{18}(r, \lambda) \sin^2\theta \cos\theta](Pr) + [f_{19}(r, \lambda) \sin^2\theta \cos\theta] + [f_{20}(r, \lambda) \sin^2\theta \cos\theta]\frac{1}{(Pr)}, \tag{11.13}$$

$$T_{2,0} = [f_{21}(r, \lambda)(1 - 3\cos^2\theta) + f_{22}(r, \lambda)] + [f_{23}(r, \lambda)(1 - 3\cos^2\theta)]\frac{1}{(Pr)}, \tag{11.14}$$

$$T_{2,1} = [f_{24}(r, \lambda)(1 - 3\cos^2\theta) + f_{25}(r, \lambda)](Pr) + [f_{26}(r, \lambda)(1 - 3\cos^2\theta) + f_{27}(r, \lambda)] + [f_{28}(r, \lambda)(1 - 3\cos^2\theta)]\frac{1}{(Pr)}, \tag{11.15}$$

and

$$\psi_{3,0} = [f_{29}(r, \lambda)(5\sin^2\theta\cos^2\theta - \sin^2\theta) + f_{30}(r, \lambda)\sin^2\theta] + [f_{31}(r, \lambda)(5\sin^2\theta\cos^2\theta - \sin^2\theta) + f_{32}(r, \lambda)\sin^2\theta]\frac{1}{(Pr)} + [f_{33}(r, \lambda)(5\sin^2\theta\cos^2\theta - \sin^2\theta) + f_{34}(r, \lambda)\sin^2\theta]\frac{1}{(Pr)^2}. \quad (11.16)$$

Every function $f_z(r, \lambda)$, $1 \leq z \leq 34$, consists of a summation of terms of the form $r^x(\ln r)^y$, where $-6 \leq x \leq 9$ and $0 \leq y \leq 2$. The coefficients of these terms are functions of the radius ratio λ only. The expressions for f_z are lengthy and are omitted here to conserve space; details may be found in the studies by Gulwadi [19].

The term $T_{0,0}$ from equation (11.1) represents the contribution to heat transfer due to pure conduction in the absence of any fluid motion, while the terms in equations (11.2–11.5) show the contribution to heat transfer by pure forced convection due to the injection/suction of fluid through the porous boundaries.

The coefficients of powers in Ra only, in equations (7) and (8), whose solutions are presented in equations (11.6), (11.9), (11.12), (11.14), and (11.16) represent the case of free convection ($Re = 0$). The remaining terms in equations (7) and (8) whose solutions are shown in equations (11.7), (11.8), (11.10), (11.11), (11.13) and (11.15) denote the interaction between free and forced convection.

The range of values of Ra and Re, for which the perturbation solution is accurate is determined by comparison with the numerical solution of the governing equations for fluid flow and energy. The numerical solution is obtained by employing a finite-difference technique to solve equations (2) and (3) subject to the boundary conditions given in equations (4.1–4.6). Using second-order finite-difference formulae to substitute for the derivatives of the dependent variables in the region $1 \leq r \leq 1/\lambda$, $0 \leq \theta \leq \pi$, we obtain a set of implicit, non-linear algebraic, finite-difference equations. The resulting set of non-linear algebraic equations is then solved iteratively by using the Newton–Raphson method.

3. Results and discussions

Flow patterns in the meridional plane for $Ra = 500$, $Pr = 0.7$, and $\lambda = 0.5$, and with increasing injection Reynolds numbers Re, are shown in Fig. 2. From Fig. 2 it is observed that in the case of pure free convection ($Re = 0$), the flow pattern consists of a clockwise rotating eddy created by the density gradient due to the temperature difference between the porous spheres (the inner being at a higher temperature than the outer). With increasing injection Reynolds numbers the eddy progressively decreases in size in the direction of the lower pole ($\theta = 180°$), until it disappears and the streamlines become more radial in nature. Flow patterns for increasing suction at the inner boundary for $Ra = 500$, $Pr = 0.7$, and $\lambda = 0.5$ are presented in Fig. 3. For increasing magnitudes of suction Reynolds numbers the eddy decreases in size in the direction of the upper pole ($\theta = 0°$), where it eventually disappears.

Variations in the radial velocity V_r, as a function of the dimensionless radial coordinate $R_r = (\bar{r} - \bar{R}_1)/(\bar{R}_2 - \bar{R}_1)$ are presented in Fig. 4 at $\theta = 180°$ for $Ra = 500$, $Pr = 0.7$, $\lambda = 0.5$,

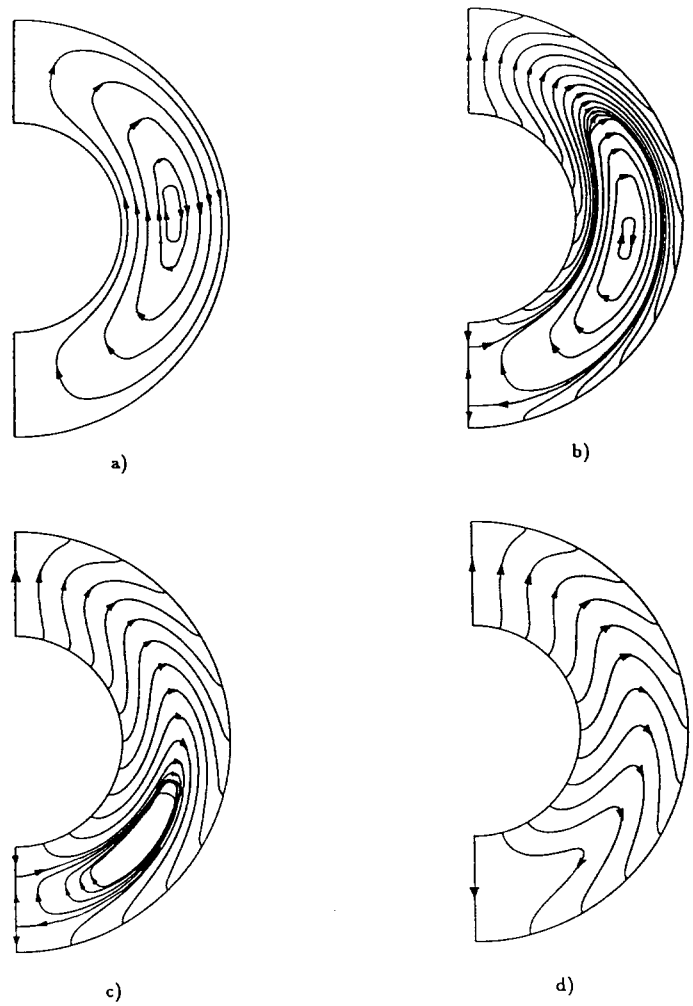

Fig. 2. Streamlines for $Ra = 500$, $Pr = 0.7$ and $\lambda = 0.5$ when *a*) $Re = 0$, b) $Re = 1$, c) $Re = 3$, and d) $Re = 5$.

and increasing values of injection Reynolds numbers. From Fig. 4 it is seen that, for relatively low values of injection Reynolds numbers, two stagnation points exist on the streamlines at $\theta = 180°$, which indicate the presence of the eddy shown in Fig. 2. The distance between the stagnation points decreases with increasing injection, signifying a decrease in the size of the eddy.

Distributions of the temperature T as a function of the dimensionless radial coordinate R_r, are shown in Fig. 5 at $\theta = 90°$ for $Ra = 500$, $Pr = 0.7$, $\lambda = 0.5$, and various values of injection/suction Reynolds numbers Re. Figure 5 shows an increase in temperature with increasing injection Reynolds numbers, and a decrease with increasing magnitudes of suction Reynolds numbers. It is also observed that injection at the inner sphere results in a decrease in the radial gradient of temperature at the inner porous wall and an increase at the outer; while suction at the inner sphere results in an opposite effect.

Heat transfer at the porous boundaries is analyzed by studying the local and overall heat transfer rates. By defining a dimensionless radial heat flux $q = \bar{q}\bar{R}_1/\bar{k}(\bar{T}_1 - \bar{T}_2)$; where $\bar{k}$ is the thermal conductivity, the local heat transfer rates at the inner and outer porous walls are given by

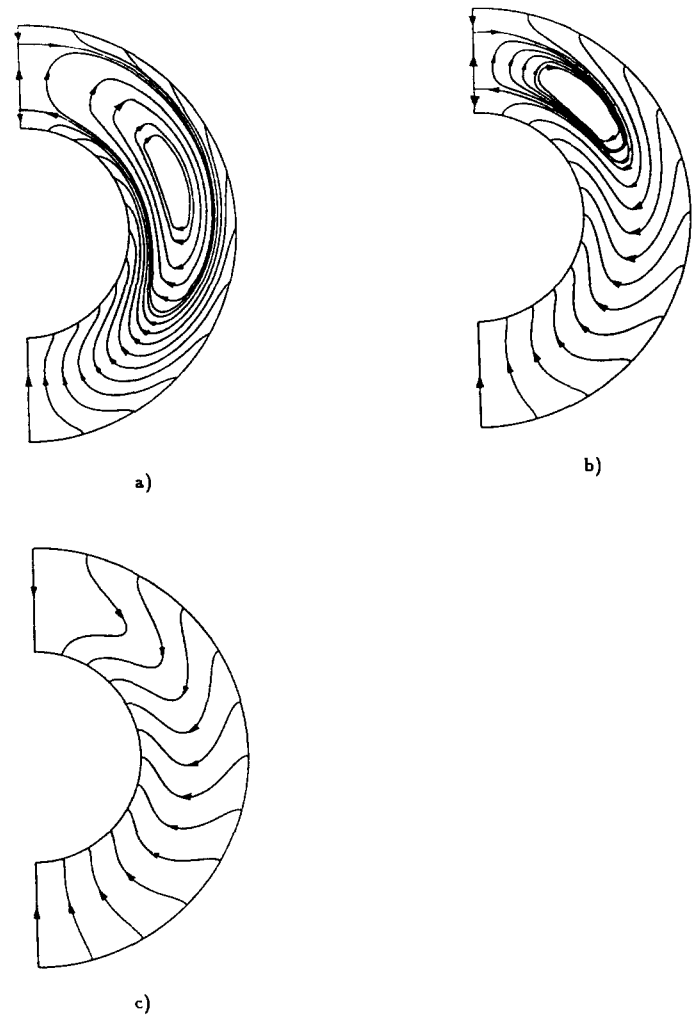

Fig. 3. Streamlines for $Ra = 500$, $Pr = 0.7$ and $\lambda = 0.5$ when a) $Re = -1$, b) $Re = -3$, and c) $Re = -5$.

$$(q)_{r=1} = \left(\frac{\bar{q}\bar{R}_1}{\bar{k}(\bar{T}_1 - \bar{T}_2)}\right)_{r=1} = -\left(\frac{\partial T}{\partial r}\right)_{r=1}, \tag{12.1}$$

and

$$(q)_{r=1/\lambda} = \left(\frac{\bar{q}\bar{R}_1}{\bar{k}(\bar{T}_1 - \bar{T}_2)}\right)_{r=1/\lambda} = -\left(\frac{\partial T}{\partial r}\right)_{r=1/\lambda}. \tag{12.2}$$

Substituting for the temperature from equation (11.1) into equations (12.1) and (12.2), the heat flux due to pure conduction at the inner and outer walls is

$$(q_c)_{r=1} = \frac{1}{(1-\lambda)}, \tag{13.1}$$

and

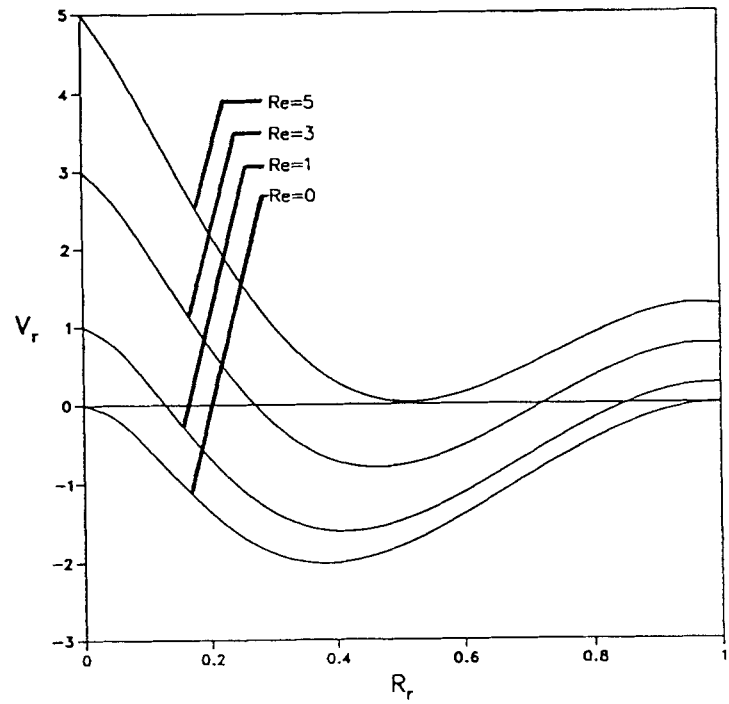

Fig. 4. Plots of radial velocity V_r vs. R_r at $\theta = 180°$ for $Ra = 500$, $Pr = 0.7$, $\lambda = 0.5$, and various injection Reynolds numbers.

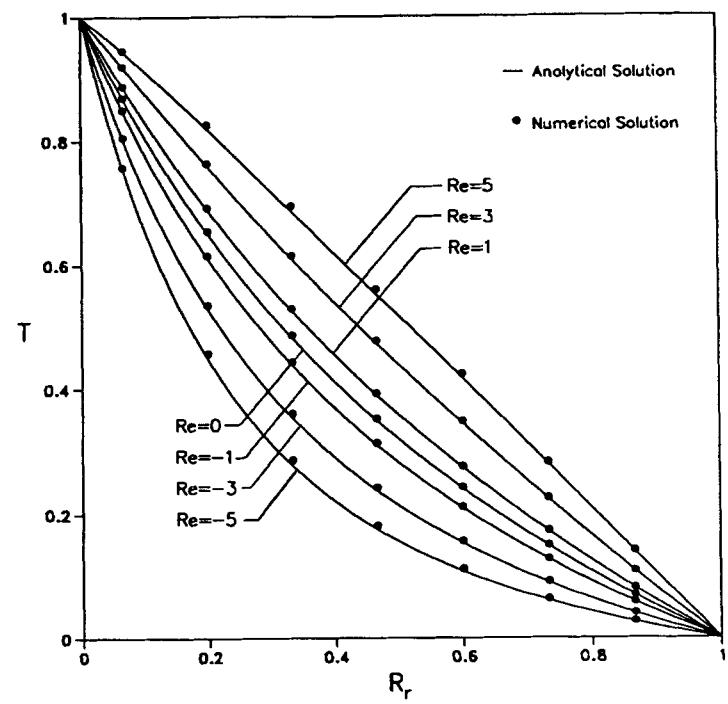

Fig. 5. Plots of temperature T vs. R_r at $\theta = 90°$ for $Ra = 500$, $Pr = 0.7$, $\lambda = 0.5$, and various injection/suction Reynolds numbers.

$$(q_c)_{r=1/\lambda} = \frac{\lambda^2}{(1-\lambda)}, \tag{13.2}$$

Combining equations (12.1), (12.2), (13.1), and (13.2), the ratio of the local radial heat flux to the radial heat flux due to pure conduction q/q_c, at the inner and outer spheres, is expressed as

$$\left(\frac{q}{q_c}\right)_{r=1} = q_1 = -(1-\lambda)\left(\frac{\partial T}{\partial r}\right)_{r=1}, \tag{14.1}$$

and

$$\left(\frac{q}{q_c}\right)_{r=1/\lambda} = q_2 = -\frac{(1-\lambda)}{\lambda^2}\left(\frac{\partial T}{\partial r}\right)_{r=1/\lambda}. \tag{14.2}$$

Figure 6 shows the variations of the local heat transfer rates at the inner and outer porous spheres as a function of θ for $Ra = 500$, $Pr = 0.7$, $\lambda = 0.5$, and increasing values of the injection Reynolds number. In the case of pure free convection ($Re = 0$), the local heat transfer rates at the inner sphere above the equator, and at the outer sphere below the equator, are lower than those values for pure conduction. Elsewhere, on the inner and outer spheres the local heat transfer rates are higher than those due to pure conduction. These results are in agreement with those obtained by Hardee [20]. With increasing injection at the

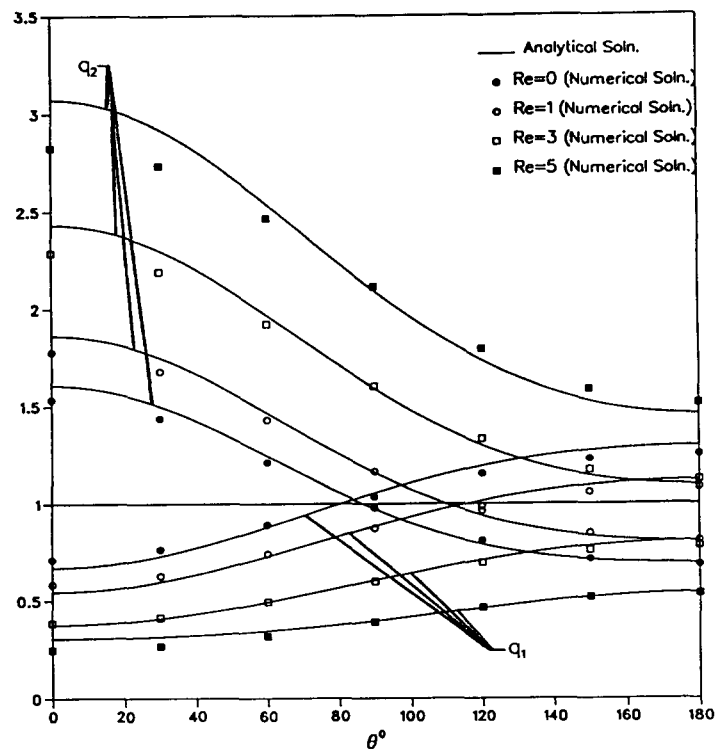

Fig. 6. Local heat transfer rates at the inner and outer porous spheres vs. θ for $Ra = 500$, $Pr = 0.7$, $\lambda = 0.5$, and various injection Reynolds numbers.

inner sphere, the local heat transfer rates at the inner sphere decrease while they increase at the outer sphere. For values of $Re = 3$ and 5, it is seen from Fig. 6 that the local heat transfer rates throughout the inner porous surface are lower than those values for pure conduction, while throughout the outer porous surface the local heat transfer rates are above those due to conduction.

By defining a dimensionless overall heat transfer rate $Q = \bar{Q}/4\pi\bar{R}_1\bar{k}(\bar{T}_1 - \bar{T}_2)$,

$$(Q)_{r=1} = \left(\frac{\bar{Q}}{4\pi\bar{R}_1\bar{k}(\bar{T}_1 - \bar{T}_2)}\right)_{r=1} = -\frac{1}{2}\int_0^{\pi}\left[r^2\frac{\partial T}{\partial r}\right]_{r=1}\sin\theta\,\mathrm{d}\theta\,, \tag{15.1}$$

$$(Q)_{r=1/\lambda} = \left(\frac{\bar{Q}}{4\pi\bar{R}_1\bar{k}(\bar{T}_1 - \bar{T}_2)}\right)_{r=1/\lambda} = -\frac{1}{2}\int_0^{\pi}\left[r^2\frac{\partial T}{\partial r}\right]_{r=1/\lambda}\sin\theta\,\mathrm{d}\theta\,. \tag{15.2}$$

Substituting equation (11.1) into equations (15.1) and (15.2), the overall heat transfer rates at the inner and outer spheres due to pure conduction are expressed as

$$(Q_c)_{r=1} = (Q_c)_{r=1/\lambda} = \frac{1}{(1-\lambda)}\,. \tag{16}$$

As a result, by combining equations (15.1), (15.2), and (16), the ratio (Q/Q_c) evaluated at the inner and outer spheres are given by

$$\left(\frac{Q}{Q_c}\right)_{r=1} = Q_1 = -\frac{(1-\lambda)}{2}\int_0^{\pi}\left[r^2\frac{\partial T}{\partial r}\right]_{r=1}\sin\theta\,\mathrm{d}\theta\,, \tag{17.1}$$

and

$$\left(\frac{Q}{Q_c}\right)_{r=1/\lambda} = Q_2 = -\frac{(1-\lambda)}{2}\int_0^{\pi}\left[r^2\frac{\partial T}{\partial r}\right]_{r=1/\lambda}\sin\theta\,\mathrm{d}\theta\,. \tag{17.2}$$

Using the analytical solution for T, the expressions for Q_1 and Q_2 are

$$Q_1 = (1 + [N_1]Re\,Pr + [N_2]Re^2\,Pr^2 + [N_3]Re^4\,Pr^4) + ([N_4] + [N_5]Re\,Pr + [N_6]Re)(Ra^2)\,, \tag{18.1}$$

and

$$Q_2 = (1 - [N_1]Re\,Pr + [N_2]Re^2\,Pr^2 + [N_3]Re^4\,Pr^4) + ([N_4] + [N_5]Re\,Pr + [N_6]Re)(Ra^2)\,. \tag{18.2}$$

The coefficients in equations (18.1) and (18.2) are functions of the radius ratio λ only, and are presented in tabular form in Table 1.

Figure 7 shows the variations of overall heat transfer rates at the inner and outer porous spheres for different values of injection and suction Reynolds numbers, at $Ra = 500$, $Pr = 0.7$, and $\lambda = 0.5$. From Fig. 7 it is seen that for increasing injection at the inner sphere (with suction at the outer), radial convective transfer of energy decreases the overall heat transfer rate at the inner porous sphere and increases it at the outer; while increasing suction at the inner sphere (with injection at the outer) results in an opposite effect. It is also observed that small rates of injection or suction can have a considerable effect on the overall

Table 1. Coefficients for overall heat transfer rates at the porous spheres

λ	N_1	N_2	N_3	N_4	N_5	N_6
0.1	−0.4500	6.75×10^{-2}	-9.11×10^{-4}	2.97×10^{-2}	1.72×10^{-2}	-2.29×10^{-3}
0.2	−0.4000	5.33×10^{-2}	-5.69×10^{-4}	5.74×10^{-4}	2.21×10^{-4}	-3.63×10^{-5}
0.3	−0.3500	4.08×10^{-2}	-3.33×10^{-4}	2.77×10^{-5}	7.21×10^{-6}	-1.31×10^{-6}
0.4	−0.3000	3.00×10^{-2}	-1.80×10^{-4}	1.78×10^{-6}	3.07×10^{-7}	-5.93×10^{-8}
0.5	−0.2500	2.08×10^{-2}	-8.68×10^{-5}	1.19×10^{-7}	1.30×10^{-8}	-2.60×10^{-9}
0.6	−0.2000	1.33×10^{-2}	-3.56×10^{-5}	6.74×10^{-9}	4.39×10^{-10}	-8.98×10^{-11}
0.7	−0.1500	7.50×10^{-3}	-1.13×10^{-5}	2.59×10^{-10}	8.85×10^{-12}	-1.83×10^{-12}
0.8	−0.1000	3.33×10^{-3}	-2.22×10^{-6}	4.25×10^{-12}	6.09×10^{-14}	-1.12×10^{-14}
0.9	−0.0500	8.33×10^{-4}	-1.39×10^{-7}	7.42×10^{-15}	2.55×10^{-17}	5.37×10^{-17}

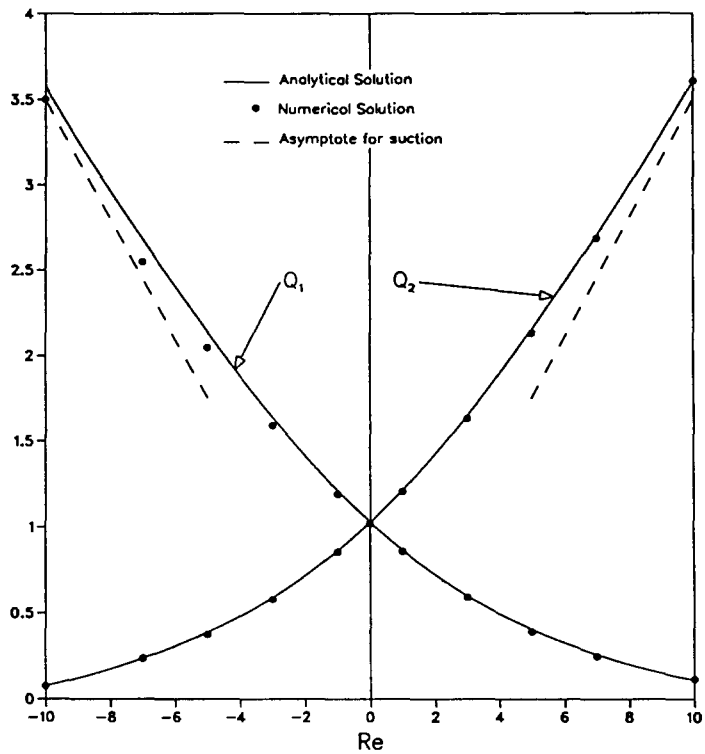

Fig. 7. Overall heat transfer rates at the inner and outer porous spheres for $Ra = 500$, $Pr = 0.7$, $\lambda = 0.5$, and increasing magnitudes of injection/suction Reynolds numbers.

heat transfer rates at the porous walls. As an example, for $Ra = 500$, $Pr = 0.7$, and $\lambda = 0.5$, the overall heat transfer rate at the outer sphere increases by 60% while it decreases by 42% at the inner sphere, when the injection Reynolds number Re is increased from a value of 0 to 3.

For large rates of injection or suction at the porous walls, the effects of free convection are negligible when compared to forced convection, with the temperature and velocity fields being dependent only on the radial coordinate r. In the case of forced convection between concentric porous spheres where the effects of free convection have been neglected, the following expression for T has been provided by Bird et al. [21],

$$T = \frac{e^{-Re\ Pr/r} - e^{-Re\ Pr\ \lambda}}{e^{-Re\ Pr} - e^{-Re\ Pr\ \lambda}}. \tag{19}$$

Substituting for T from equation (19) into equations (17.1) and (17.2), we get

$$Q_1 = \frac{(1-\lambda)Re\ Pr}{e^{Re\ Pr(1-\lambda)} - 1}, \tag{20.1}$$

and

$$Q_2 = \frac{(1-\lambda)Re\ Pr}{1 - e^{-Re\ Pr(1-\lambda)}}. \tag{20.2}$$

For increasing injection at the inner porous sphere (with suction at the outer), we observe from equations (20.1) and (20.2) that, as $Re \to \infty$; $Q_1 \to 0$ asymptotically, while $Q_2 \to (1-\lambda)Re\ Pr$ asymptotically. In the case of increasing suction at the inner porous sphere (with injection at the outer), from equations (20.1) and (20.2), it is noted that as $Re \to -\infty$; $Q_2 \to 0$, while $Q_1 \to (1-\lambda)Re\ Pr$. The asymptotic behavior of heat transfer results for increasing injection or suction at the porous spheres can be seen in Fig. 7.

Figure 8 shows the variation of Q_1 with increasing values of the Rayleigh number for $Pr = 0.7$, $\lambda = 0.5$, and various values of injection/suction Reynolds numbers. From Fig. 8 it is seen that the effects of free convection increase with increasing values of Ra. However, for

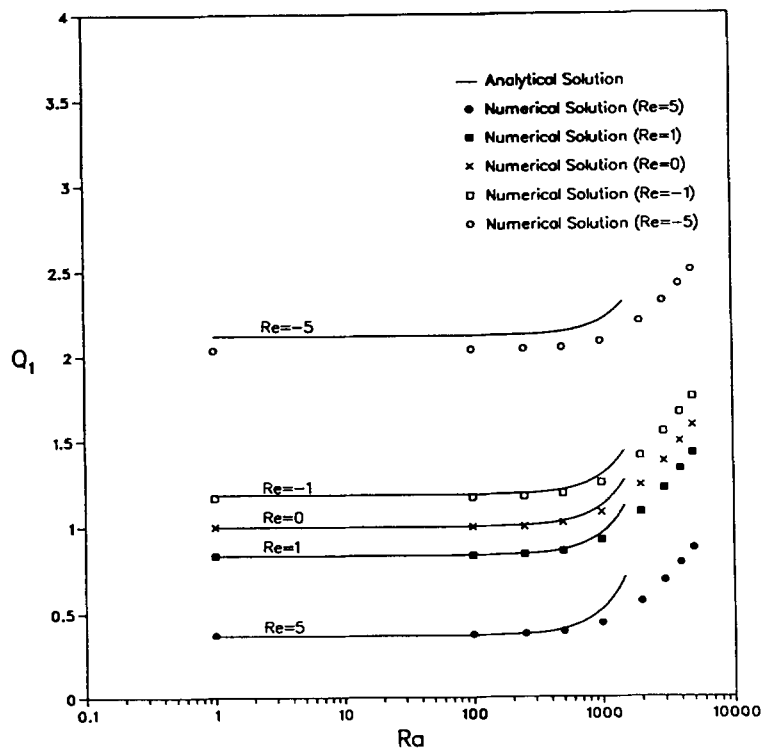

Fig. 8. Plots of overall heat transfer rate at the inner porous sphere vs. Ra for $Pr = 0.7$, $\lambda = 0.5$, and various injection/suction Reynolds numbers.

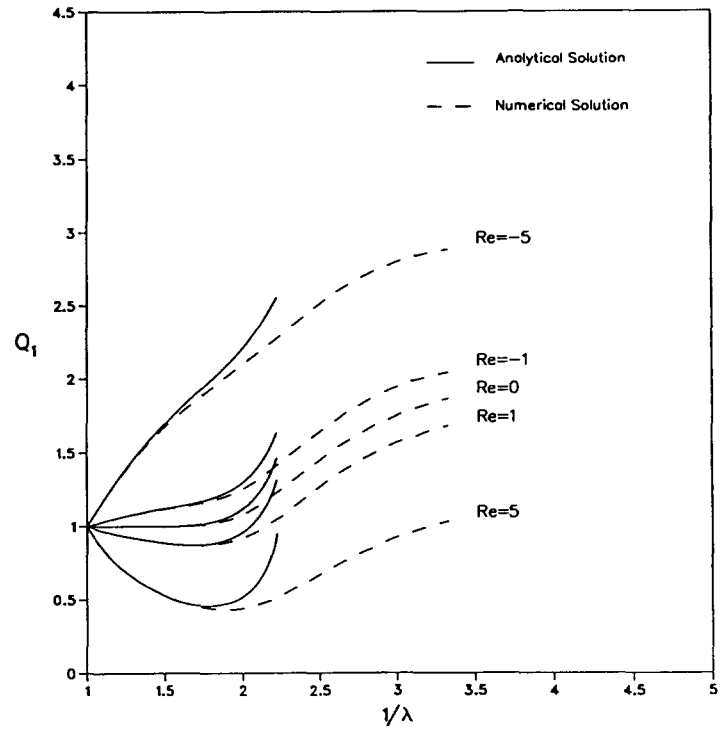

Fig. 9. Plots of overall heat transfer rate at the inner porous sphere vs. $1/\lambda$ for $Ra = 1000$, $Pr = 0.7$, and various injection/suction Reynolds numbers.

values of $Ra \leqslant 250$, approximately, the effects of free convection are negligible; which is in agreement with the results of Astill et al. [3] for $Re = 0$. It is also observed from Fig. 8 that the analytical and numerical results show good agreement in the range $|Re| \leqslant 5$ and $Ra \leqslant 1000$, approximately.

Figure 9 shows the plot of Q_1 with increasing values of $1/\lambda$ for $Pr = 0.7$, $Ra = 1000$, and various values of injection/suction Reynolds numbers. Comparisons between the analytical and numerical results, from Fig. 9, indicate that for a value of $\lambda = 0.5$ there is good agreement between the two solutions in the range $|Re| \leqslant 5$, approximately.

4. Conclusions

In this investigation, the effects of transpiration on free convection in an annulus between concentric porous are studied by employing a regular perturbation technique. Results are presented over a range of values for the Rayleigh number Ra and injection/suction Reynolds number Re, where the strength of the radial flow-field is comparable to that of free convection flow. The stream-line plots and velocity distributions for a constant value of Ra and increasing injection/suction rates display the transition of flow from a circulatory flow-pattern for pure free convection ($Re = 0$) to a radial flow-pattern where the effects of forced convection are dominant. Heat transfer results at the porous spheres also indicate that for a given value of Ra and increasing rates of injection/suction, the combined effects of free

and forced convection are significant over a range of values of *Re*, beyond which the effects of free convection are negligible.

Results from a numerical solution of the governing equations for fluid flow and energy using a finite-difference scheme are also provided in this study. The range of values of *Ra* and *Re* for which the analytical solution is valid is determined by comparison with the numerical solution.

References

1. L.R. Mack and H.C. Hardee, Natural convection between concentric spheres at low Rayleigh numbers. *Int. J. Heat Mass Transfer* 11 (1968) 387–396.
2. S.N. Singh and J. Chen, Numerical solution for free convection between concentric spheres at moderate Grashof numbers. *Numer. Heat Transfer* 3 (1980) 441–459.
3. K.N. Astill, H. Leong and R. Martorana, A numerical solution for natural convection in concentric spherical annuli. Presented at the 19th. National Heat Transfer Conference, Orlando, Fla., HTD-8 (1980) 105–113.
4. J.-P. Caltagirone, M. Combarnous and A. Mojtabi, Natural convection between two concentric spheres: transition towards a multicellular flow. *Numer. Heat Transfer* 3 (1980) 107–114.
5. D.B. Ingham, Heat transfer by natural convection between spheres and cylinders. *Numer. Heat Transfer* 4 (1981) 53–67.
6. V.K. Garg, Natural convection between concentric spheres. *Int. J. Heat Mass Transfer* 35 (1992) 1935–1945.
7. E.H. Bishop, L.R. Mack and J.A. Scanlan, Heat transfer by natural convection between concentric spheres. *Int. J. Heat Mass Transfer* 9 (1966) 649–662.
8. J.A. Scanlan, E.H. Bishop and R.E. Powe, Natural convection heat transfer between concentric spheres. *Int. J. Heat Mass Transfer* 13 (1970) 1857–1872.
9. S.H. Yin, R.E. Powe, J.A. Scanlan and E.H. Bishop, Natural convection flow patterns in spherical annuli. *Int. J. Heat Mass Transfer* 16 (1973) 1785–1795.
10. F.-S. Lien, C.-K. Chen and J.W. Cleaver, Mixed and free convection over a rotating sphere with blowing and suction. ASME *J. Heat Transfer* 108 (1986) 398–404.
11. P. Hatzikonstantinou, Unsteady mixed convection about a porous rotating sphere. *Int. J. Heat Mass Transfer* 33 (1990) 19–27.
12. S.D. Gulwadi, A.F. Elkouh and T.-C. Jan, Laminar flow in an annulus between two concentric rotating porous spheres. *Acta Mechanics* 97 (1993) 215–228.
13. R. Eichhorn, The effect of mass transfer on free convection. *ASME J. Heat Transfer* 82C (1960) 260–263.
14. E.M. Sparrow and R.D. Cess, Free convection with blowing and suction. *ASME J. Heat Transfer* 81C (1961) 387–389.
15. J.H. Merkin, Free convection with blowing and suction. *Int. J. Heat Mass Transfer* 15 (1972) 989–999.
16. J.F. Clarke, Transpiration and natural convection-vertical flat plate problem. *J. Fluid Mech.* 57 (1973) 45–61.
17. P.G. Parikh, R.J. Moffat, W.M. Kays and D. Bershader, Free convection over a vertical porous plate with transpiration. *Int. J. Heat Mass Transfer* 17 (1974) 1465–1474.
18. T. Watanabe, Free convection boundary layer flow with uniform suction or injection over a cone. *Acta Mechanica* 87 (1991) 1–9.
19. S.D. Gulwadi, Effects of transpiration on free convection in an annulus between concentric porous spheres. *Ph.D. Dissertation*, Marquette University (1993).
20. H.C. Hardee, Natural convection between concentric spheres at low Rayleigh numbers. *Ph.D. Dissertation*, University of Texas (1966).
21. R.B. Bird, W.E. Stewart and E.N. Lightfoot, *Transport Phenomena*, New York, Wiley (1960) 328–330.